Commun. Comput. Phys.
doi: 10.4208/cicp.OA-2015-0015

Vol. **21**, No. 2, pp. 466-489
February 2017

Numerical Study of the Solid Particle Erosion on H-Type Finned Circular/Elliptic Tube Surface

Yu Jin, Gui-Hua Tang, Ya-Ling He and Wen-Quan Tao*

Key Laboratory of Thermo-Fluid Science & Engineering,School of Energy and Power Engineering, Xi'an Jiaotong University, Xi'an, Shaanxi 710049, China.

Communicated by Boo-Cheong Khoo

Received 24 November 2015; Accepted (in revised version) 23 August 2016

Abstract. In this paper, numerical simulations of solid particle erosion phenomena on H-type finned circular/elliptic tube surface, which is of great significance to the anti-wear design of heat exchanger, are presented. The Eulerian-Lagrangian approach is applied to simulate the dilute gas-solid flow through H-type finned circular/elliptic tubes. A semi-empirical model is adopted to predict the erosion rate. The dynamics behavior of the entrained solid particles in the flow is presented. The geometry of eroded tube surface is changed with the predicted erosion which is taken into account by a UDF and the flow field is re-solved for the eroded tube surface at every time step. The influences of ten parameters (the tube bundle arrangement, particle size, particle concentration, fluid Reynolds number, fin thickness, fin pitch, fin length, fin width, slit width and the transverse tube pitch) on the maximum erosion depth of the H-type circular/elliptic finned tube surface are investigated. Using H-type finned elliptic tube surface can effectively reduce the erosion rate of tube surface compared with that using H-type finned circular tube surface. The erosion in in-line arrangement is less severe than that in staggered arrangement. With the increase of particle size, particle concentration and the fluid Reynolds number, the erosion rate of the tube surface rises. The numerically predicted effect of Reynolds number is in good agreement with previous test data. Among the six geometry parameters, the most influential parameter is the transverse tube pitch.

AMS subject classifications: 80A20, 76Fxx

Key words: Waste heat recovery, H-type finned circular/elliptic tube, solid particle erosion, numerical simulation.

1 Introduction

In coal-fired power plants, a mass of fly ash would be produced due to the burning of pulverized coal in the boiler burners. When the high temperature gas mixed with ash

*Corresponding author. *Email address:* wqtao@mail.xjtu.edu.cn (W.-Q. Tao)

particles flows over tube bank, the heat exchangers have to be operated in contaminated environments. The ash particles collide with the surface of the heat exchanger tubes, thus the material surface is eroded. At the most severe situation, the tube walls can be perforated, which leads to a significant reduction of the tubes' performance life. Therefore, the study on erosion process and erosion characteristics of dusty gas flowing across heat exchanger tube bundle is of great importance.

Solid particle erosion of surface is a micromechanical process that is influenced by numerous factors, including flow condition, tube bank geometry, target material, particle size and shape, particle velocity, impact angle and fluid properties. Many experiments have been conducted on the wear of a surface through the solid particle erosion. Early in the 1960 Finnie [1] experimentally studied the erosion by solid particles on different surface materials, and the results indicate that the effects of particle velocity and impact angle on the erosion of a brittle material and a ductile material are very different. The first erosion model was proposed based on his experimental results. Later, Tabakoff et al. [2] carried out the experiments to study the erosion of coal ash particles on different alloys and presented a new erosion model, which is widely adopted to predict the erosion rate of surface by coal ash particles. Bauver et al. [3] carried out well-defined experiments to predict the erosion of boiler tube and obtained the detailed erosion distribution on tube surface. Schade et al. [4] designed a test facility to investigate the characteristics of particle-wall impact and measured the restitution coefficient and friction coefficient of the particle-wall impact by this experimental setup. Li et al. [5] experimentally investigated the wear characteristics of three types of heat transfer tubes with special nickel infiltration layers and suggested that the application of this tube may effectively improve the working life of heat transfer equipment in high temperature dusty gas flows. Deng et al. [6] studied particle rotation's effects on the erosion rate of metals and proposed that the rotation direction of the angular particles has a most important effect on the erosion rate of the target materials at low impact angles. With the development of computer technology, numerical research has become an important method of erosion prediction. The numerical studies on erosion rate of heat exchanger tube bundle were widely conducted. Fan et al. [7] numerically investigated the collision frequency of coal particle and the erosion distribution of bare tube surface and claimed that the numerical results were in good agreement with the experiment data. Tu et al. [8] adopted the two-fluid turbulence model with a developed particle-wall collision model to predict the trajectories of fly-ash particles in power utility boilers and proved that the Stokes number of particles has a significant effect on the particle distribution character. Fan et al. [9] numerically studied the particle collision and bare tube erosion characteristics and suggested that the fixing fins on tubes can easily and efficiently reduce the erosion damage of tube. Lee et al. [10] numerically studied the fly-ash erosion of single tube by the Eulerian approach and the numerical results are in good agreement with experimental data. Jin et al. [11] conducted numerical simulations to investigate the erosion characteristics of two-row bare tubes and obtained particle collision and erosion distributions of tube surface. Lee et al. [12] adopted both the Eulerian and Lagrangian methods to study the particle flow

and tube erosion characters and observed that the results predicted by both approaches were in good agreement. Tian et al. [13] investigated the physical behaviour of a dilute gas-particle flow along an in-line tube bank and applied the Lagrangian particle-tracking model to study the characteristics of the particle-wall collisions. They suggested that for large particles the particle fluctuations were mainly determined by the particle-wall collisions. Liu and Hinrichsen [14] numerically studied the bare tube erosion in a bubbling fluidized bed and analysed the effect of the bubble behaviors on erosion rate. They proposed that the variation of particle-wall restitution coefficient does not lead to an evident change in the erosion rate of tube surface. Wang et al. [15,16] performed numerical simulations to study the particle trajectories in a 10×10 aligned tube bank and mainly investigate the impact and erosion characteristics on the stainless steel bare tubes. Zhao et al. [17,18] numerically studied the heat transfer and erosion characteristics of the single H-type finned elliptic tube with enhanced heat transfer structures and the results showed that the H-type finned elliptic tube with LVG structure has a good anti-wear performance. In the study or research above, the deformation of tube surface with the impacting process was not considered.

Although much work has been done on simulation of erosion of heat exchanger tube surface, the recent literature mainly focused on gas-particle flow across simple cylinder, simple tube bank made of smooth tubes, without considering the deformation of tube surface. Given that the heat transfer surface gradually changes during the erosion process, taking the deformation of tube surface into account is much more accurate and intuitional to present the erosion of tube surface. In the waste-heat recovery heat exchangers H-type finned circular/elliptic tube as shown in Fig. 1 has been widely used because of its good anti-wear and anti-fouling performance provided by its unique groove structure in fin surface. However, few studies have been conducted on it by now, so it is necessary to conduct systematic numerical study on the erosion of H-type finned tube with the consideration of the deformation of tube surface.

In this paper, numerical simulation of solid particle erosion phenomena on the H-type finned circular/elliptic tube surface is performed by software FLUENT [19]. The geometry of eroded tube surface is changed with the predicted erosion which is taken into account by a UDF and the flow field is re-solved for the eroded tube surface at every time step which are believed to be more accurate for erosion study. The effects of ten factors: the tube bundle arrangement, particle size, particle concentration, fluid Reynolds number, fin thickness, fin pitch, fin length, fin width, slit width and the transverse tube pitch on erosion of the H-type finned circular/elliptic tube surface are examined in detail. In the following sections, the physical model and numerical method will be firstly introduced, and the effects of ten factors are then presented in detailed numerical results. Lastly some conclusions will be presented.

2 Model description and numerical method

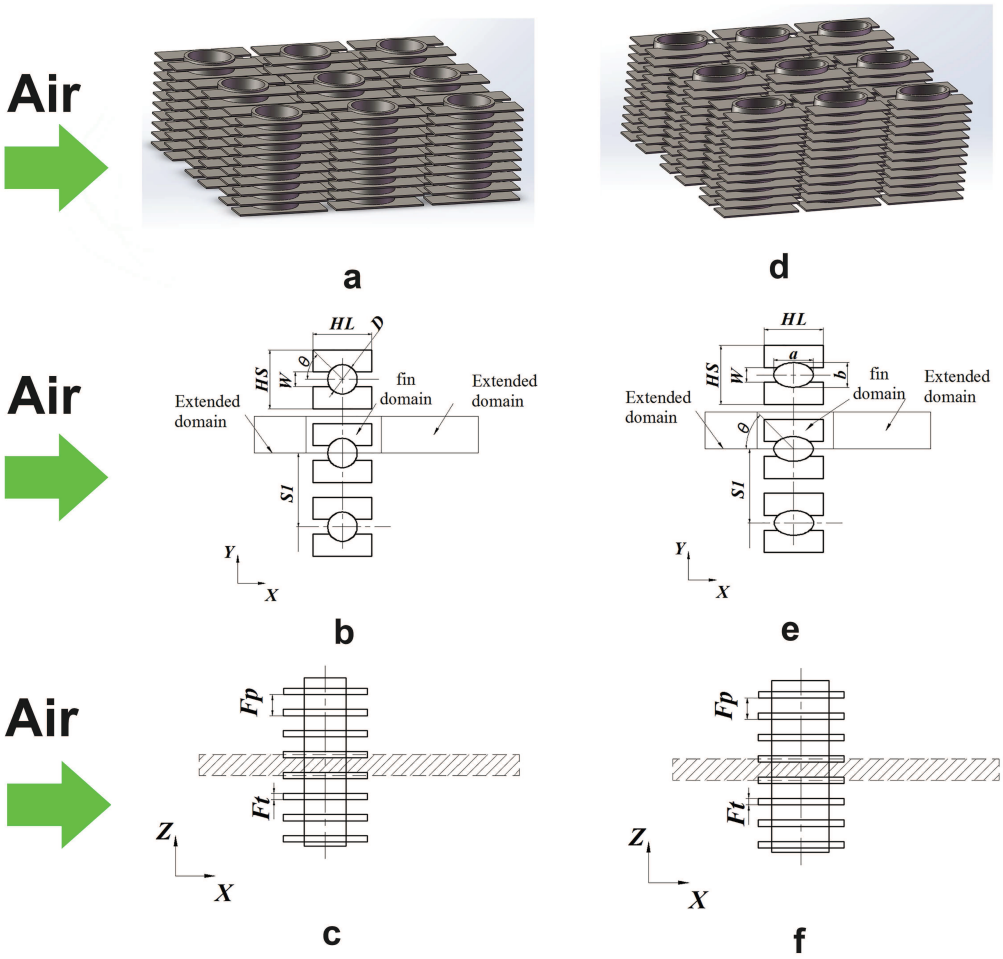

Figure 1: A schematic diagram of a single row H-type finned tube surface.

2.1 Physical model

Schematic diagrams of H-type finned circular/elliptic tube surface are shown in Fig. 1. Figs. 1(b) and (e) give top views of the computation domains of the single-row H-type finned circular/elliptic tube respectively. Figs. 1(c) and (f) present the side views of the computational domains indicated by shading, and the top and bottom are the symmetrical lines of the two neighbouring fins. It should be noted that the oncoming flow is normal to the tube axis and parallel to the long side of the H-type fins. For the convenience of numerical treatment, the actual computation domains indicated by shading in Figs. 1(c) and (f) are extended by five times and ten times each of the diameter of heat transfer tube in the entrance and outlet sections, respectively, to make sure the inlet uniformity and avoid the outlet velocity with a recirculation flow in the outlet region.

2.2 Governing equations

For gas-particle flows with particle volume fraction less than 0.001, which is usually the case of gas flow from boiler combustor, the Eulerian-Lagrangian approach [19] is widely applied to predict the dilute gas-solid flow. The turbulent fluid flow is solved as a continuous phase by calculating transport equations [20], while all the particles treated as the discrete phase in the flow field are tracked by solving the particle motion equation.

The fluid flow in the H-type finned circular/elliptic tube surface is assumed to be incompressible with constant property and unsteady with turbulence. For turbulence simulation, the RNG k-ε turbulence model [21] is adopted. The governing equations for the mass, momentum and energy conservation and for k and ε can be found in many references [20] and are not presented here for simplicity.

In addition to solving transport equations for the continuous phase, the discrete phase in the Lagrangian reference frame is also simulated by software FLUENT. In this study, the particles are considered spherical because small fly ash particles have a spherical shape in general [10]. The gas-particle flow is in the dilute region, so collision between particles is neglected. The discrete phase can exchange momentum with the continuous phase. The trajectory of the dispersed phase in a Lagrangian reference frame can be solved by integrating the force balance on the particle. The particle motion equation can be expressed as follow [19],

$$\frac{du_p}{dt} = F_D\left(U-u_p\right) + \frac{g(\rho_p-\rho)}{\rho_p} + F_{other}, \tag{2.1}$$

where the first term on the right hand side represents the drag force per unit particle mass, u_p is the particle velocity, ρ_p is the particle density, and F_D is determined as

$$F_D = \frac{18\mu}{\rho_p D_p^2}\frac{C_D Re_p}{24}, \tag{2.2}$$

where D_p is the particle diameter. Re_p is the relative Reynolds number, which is defined as

$$Re_p = \frac{\rho D_p\left|u_p-U\right|}{\mu}. \tag{2.3}$$

In Eq. (2.1) F_{other} represents other forces acting on the particle. Here only the Saffman lift force is considered according to the force analysis conducted by Cen and Fan [22]. The Saffman force F_S [23] is defined as

$$F_S = 1.615\mu D_p^2\sqrt{\frac{k_r}{\nu}}(U-u_p), \tag{2.4}$$

where k_r is the local velocity gradient.

The dispersion of particles caused by fluid turbulence can be predicted by using the stochastic tracking model. In this model, the prediction of particle dispersion applied the

concept of the integral time scale, which is the time spent in turbulent motion along the particle path. For small particles that are easily entrained by the fluid flow due to their low inertia, the integral time becomes the fluid Lagrangian integral time, T_L. The integral time scale can be approximately defined as [19]

$$T_L \approx 0.15\frac{k}{\varepsilon}. \tag{2.5}$$

2.3 Impact and rebound phenomenon of particles

When particles impact on a surface, most of them are rebounded. Tabakoff et al. [2] conducted experiments to study the rebound characteristics of the coal ash particles colliding with the stainless steel surface and proposed the expressions of the normal and tangential restitution ratios based on the experimental results. In the present work, the restitution ratios are applied and expressed by following equations [2]:

$$\frac{u_{n2}}{u_{n1}} = 1.0 - 0.4159\beta - 0.4994\beta^2 + 0.292\beta^3, \tag{2.6}$$

$$\frac{u_{t2}}{u_{t1}} = 1.0 - 2.12\beta + 3.0775\beta^2 - 1.1\beta^3, \tag{2.7}$$

where u represents the particle impact velocity. Subscripts n and t represent normal direction and tangential direction, respectively. Subscripts 1 and 2 represent the condition before and after collision, respectively. β is the collision angle between the incident velocity and the tangent to the rough surface.

Because of the considerable effects of wall roughness on the rebound behaviors of the large particles, both the particles' trajectories downstream and particle collision frequency distribution on the tubes [13] are significantly affected. Here the wall roughness effect should be taken into consideration. The collision angle between the particle and the rough surface can be defined as [24]:

$$\beta = \beta' + \Delta\gamma\xi, \tag{2.8}$$

where the β' is the collision angle between the particle and a smooth surface, ξ is a Gaussian random variable, $\Delta\gamma$ is the effect of wall roughness determined by experiment. In this study, $\Delta\gamma$ is taken as 5.3°. It is interesting to note that Tabakoff rebound model is widely used in literatures [7, 9, 11, 15–18]. Even though it does not consider the effect of temperature, it is estimated that the temperature effect of the normal and tangential restitution ratios on the erosion results is small and this has been observed in Ref. [14].

2.4 Tube mass erosion prediction

Tabakoff et al. [2] experimentally studied the effects of particle's impact velocity and the particle's impact angle on the stainless steel erosion and proposed an empirical correlation of erosion rate of steel surface by coal ash particles based on their experimental data.

The erosion rate E is defined as the ratio of the target metal material mass loss to the impacting particle mass, which can be estimated by following equation,

$$E=K_1\left\{1+C_K\left[K_2\sin\left(\frac{90}{\beta_0}\beta\right)\right]\right\}^2 u_i^2\cos^2\beta\bullet[1-(1-0.0016u_i\sin\beta)]^2+K_3(u_i\sin\beta)^4, \quad (2.9)$$

where u_i is the impact velocity, β is the collision angle, β_0 is the maximum erosion angle, $C_K=1$ for $\beta\leq 3\beta_0$ and $C_K=0$ for $\beta>3\beta_0$, K_1, K_2 and K_3 are empirical constants. Here, for a steel surface impacted by coal ash particles, the empirical constants are set to be $\beta_0=25^\circ$, $K_1=1.505\times10^{-6}$, $K_2=0.296$ and $K_3=5.0\times10^{-12}$, respectively.

This model was used to predict erosion rate of devices in [4,9,11,17,18,25,26] and the results showed a sufficient agreement between measurement and calculation in [4, 25]. Hence this model was adopted to predict the erosion rate of H-type finned tube surface in this paper.

2.5 Deformation of tubes surface

When particles impact on a surface, whether it is flat or circular, some mass of the surface is removed because of the particle impact, hence the surface contour is gradually changed. This implies that the solid-fluid interface boundary gradually changes in the process, i.e., the interface boundary is moving with the process. In this paper, the moving boundary concept was also tested. A user defined subroutine was used to update the node coordinates when the command was given to solve the flow field. This subroutine changed the grid coordinates for the wall adjacent nodes by values equal to the penetration rate. Here the penetration rate (P) is referred to the amount of wall thickness loss per unit time, which can be expressed as follow,

$$P=\frac{E\dot{m}}{A_{cell}\rho_{wall}}, \quad (2.10)$$

where $\dot{m}$ is the particle flow rate, A_{cell} is the local cell area and ρ_{wall} is the density of the tube material.

In this paper, the erosion model and the deformation of the wall were dealt by using user defined functions (UDF) in the commercial CFD software, FLUENT 6.3.26. User defined memory locations (UDML) were used to store the results in order to enable post-processing of the results and images of erosion.

2.6 Boundary conditions

At the upstream boundary, the fluid entering the computational domain is assumed to have uniform velocity and turbulent intensity with the velocity components in the y and z directions being zero. The fluid region comprises of the entrance, outlet and bundle zone and the solid region includes the fin. At the tube surface all velocity components

Table 1: Summary of the basic prediction conditions.

Parameter	Values	Parameter	Values
Tube diameter, D (mm)	42	Spanwise tube pitch, $S1$ (mm)	84
Larger ellipse diameter, a (mm)	52.5	Tube material	Carbon steel
Smaller ellipse diameter, b (mm)	30	Tube density, ρ_w (kg/m^3)	7750
Fin pitch, Fp (mm)	9	Particle density, ρ_p (kg/m^3)	1500
Fin length, HL (mm)	76.5	Fluid inlet velocity, U_{in} (m/s)	5
Fin width, HS (mm)	54	Particle diameter, D_p (μm)	50
Fin thickness, Ft (mm)	1.5	Particle flow rate, m (g/s)	0.05
Slit width, W (mm)	10	Particle concentration, C (g/m^3)	26

are set to be zero. The outlet boundary is the pressure boundary condition. The top, bottom, front and back surfaces of the computational domain are symmetrical boundary, at which the normal first derivative of velocity components parallel to the surface are zero, while that normal to the surface is zero. Details of the basic prediction conditions are listed in Table 1.

2.7 Calculation procedure of particle erosion rate

The erosion calculations performed in this study are based on the flow chart given in Fig. 2. The first step is the solution of the flow field for the given geometry by using the specified inlet and the outlet boundary conditions and the appropriate fluid flow models. Then the particles are distributed and injected at the inlet to the geometry. The particle trajectories are calculated using the Lagrangian dispersion model. Next the erosion model is applied to the particles hitting the surface in order to calculate the actual rate of particle erosion. With the predicted erosion, the geometry of the correspondent location is changed at every time step. The flow field is re-solved for the eroded surface to take into account the time dependent particle erosion. The calculations are continued until the required number of operating hours is achieved. In this paper, the time step for the flow calculation was 1×10^{-3}s, and in order to accelerate the deformation of tube surface and reduce the calculation time the penetration depth of each time step is magnified 5×10^7 times. It should be noted that after the prediction of every time step the new surface of the impacted tube is reformed and a correspondent grid system was generated to match the deformation of the tube surface.

2.8 Grid independent solution

The foregoing governing equations and the particle erosion rate are solved by the commercial code FLUENT. The grid systems are established using the preprocessor GAMBIT. The computation domains are meshed with tetrahedral elements. In the region adjacent to the solid region much finer grid distribution is used and the coarse grids are used in the extended regions to save the computing resource.

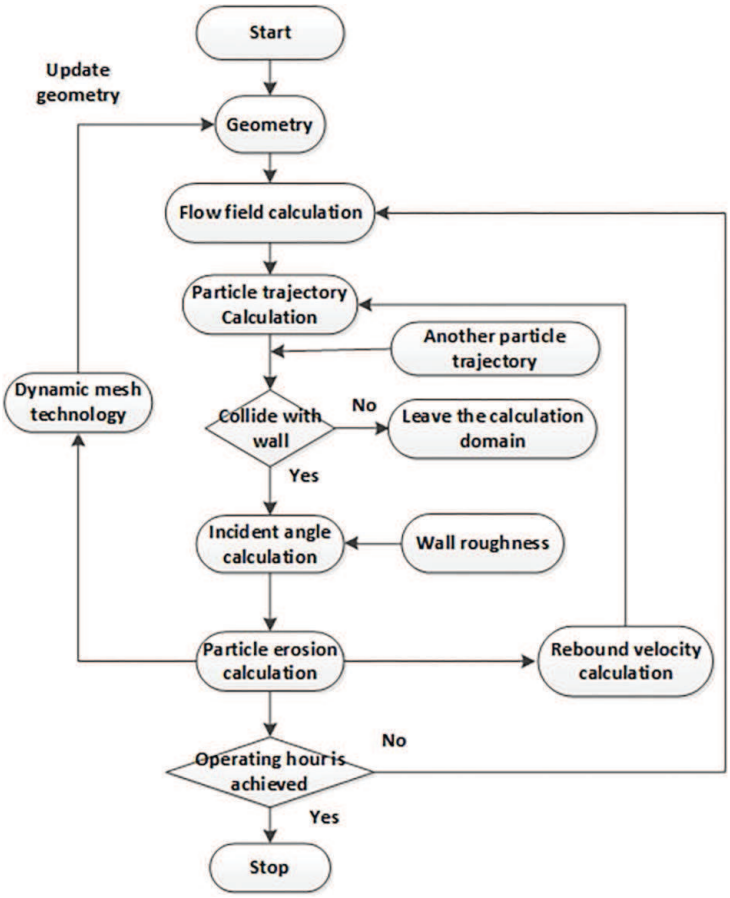

Figure 2: Flow chat of particle erosion rate calculation.

To examine the grid independence of the numerical solution, eight different grid systems are selected. The numerical calculations are carried out with 10000 time steps and the predicted pressure drop and the maximum penetration depth of the single row H-type finned circular/elliptic tube from the eight grid systems are presented in Fig. 3. From Fig. 3 it can be seen that the solution of the grid system of 359 000 and 350 000 can be regarded grid-independent for H-type finned circular/elliptic tube respectively. These two grid systems are adopted in our computation.

3 Numerical results and discussion

3.1 The deformation of tube surface

First, a general picture of the erosion caused by particle impact on a tube wall and fin surface is described. It is interestingly noteworthy that when particle-laden fluid flow

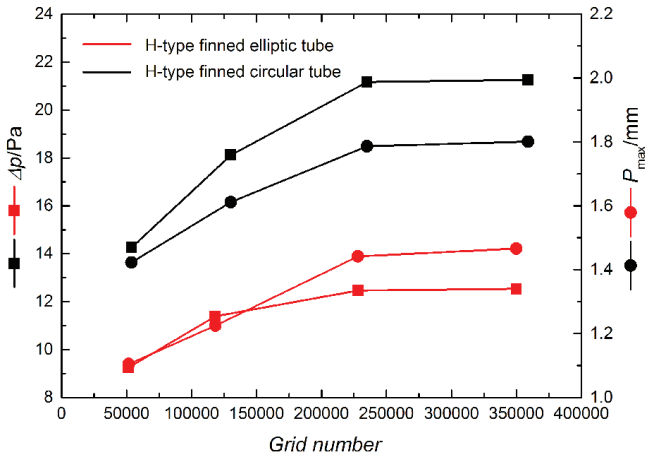

Figure 3: Variations of the predicted pressure drop and the maximum penetration depth and with grid number systems.

across H-type finned tube, the erosion rate on the fins is much less than that on the tube surface, because the direction of the air flow is nearly parallel to the fins. In addition the erosion of tube surface has a greater effect on the operation of heat exchanger than the erosion of fins does. Thus study on the erosion of the H-type finned circular/elliptic tube surface should be focused on the tube surface. The erosion of tube surface of H-type finned circular/elliptic tube at different operating time is presented in Fig. 4. The fluid inlet velocity is 7m/s and the other parameters remained the same as the basic prediction conditions in Table 1. It can be observed that with the time passes, the deformations of tube surface become progressively severe and the erosion mainly occurs at the front half of tube surface. The maximum erosion mainly locates at about the center of two adjacent fins. The variations of maximum penetration depth with the operating time are provided in Fig. 5. It can be seen that the maximum penetration depth of H-type finned circular tube surface is much deeper than that of H-type finned elliptic tube surface and the maximum penetration depths of both tube surfaces increase linearly with time. Fig. 6 presents that the locations of maximum penetration depth also increase with time and the increasing tendencies are weakened gradually, where θ is the tube angle between the incoming flow direction and the line connecting erosion location and tube center. The maximum erosion of H-type finned circular tube surface occurs at about 40° of tube angle from forward stagnation point, which proves quite good agreement with experimental results in Ref. [3]. For the H-type finned elliptic tube surface, the maximum erosion occurs at about 12° of tube angle from forward stagnation point.

From engineering viewpoint, the maximum erosion depth is the most important parameter to characterize the solid erosion by particle impact. In the following section, the effects of ten parameters on the maximum erosion depth of the H-type finned circular/elliptic tube surface are analyzed. Among these are tube bundle arrangement, parti-

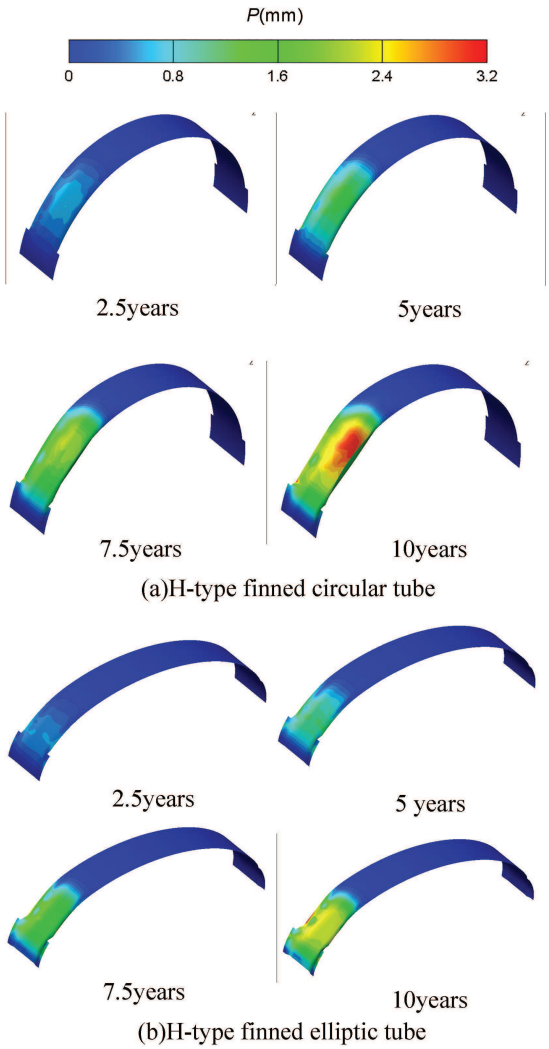

Figure 4: The deformation of H-type finned circular/elliptic tube surface at different operation time.

cle size, particle concentration, fluid Reynolds number, fin thickness, fin pitch, fin length, fin width, slit width and transverse tube pitch. The maximum erosion depth presented below is obtained after an operation time period of 15.8 years.

3.2 The effects of the ten parameters on the maximum erosion depth

3.2.1 The effect of the tube bundle arrangement

In order to examine the effects of tube bundle arrangement on the maximum penetration depths of tube surface, three kinds of tube bundle: an in-line tube bundle, a row

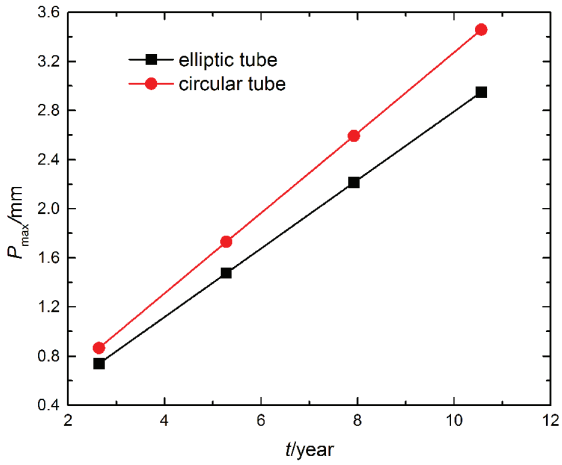

Figure 5: The variations of maximum penetration depth with the operation time.

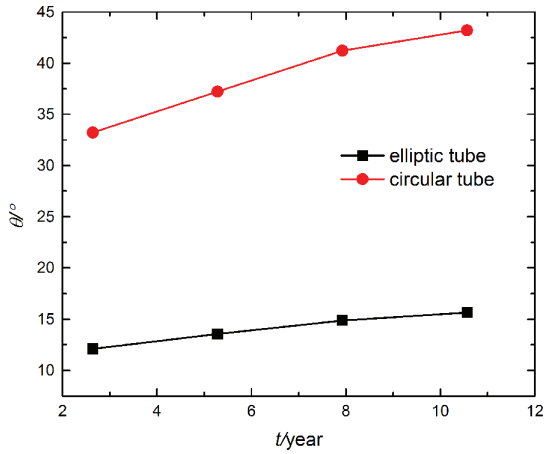

Figure 6: The variations of the location of maximum erosion with the operation time.

staggered tube bundle and a column staggered tube bundle are investigated separately. The schematic views of three H-type finned circular tube bundles are shown in Fig. 7. Though the column staggered tube bundle looks very similar to the traditional row staggered tube bundle in form, there are essential differences between them in transverse tube pitch and longitudinal tube pitch. For the traditional row staggered tube bundle, the transverse tube pitch and the longitudinal tube pitch must be greater than or equal to the tube diameter. For the column staggered tube bundle, the transverse tube pitch must be great than or equal to twice the tube diameter. The geometric parameters of the three tube bundles are listed in Table 2. The other parameters remained the same as the basic prediction conditions in the Table 1.

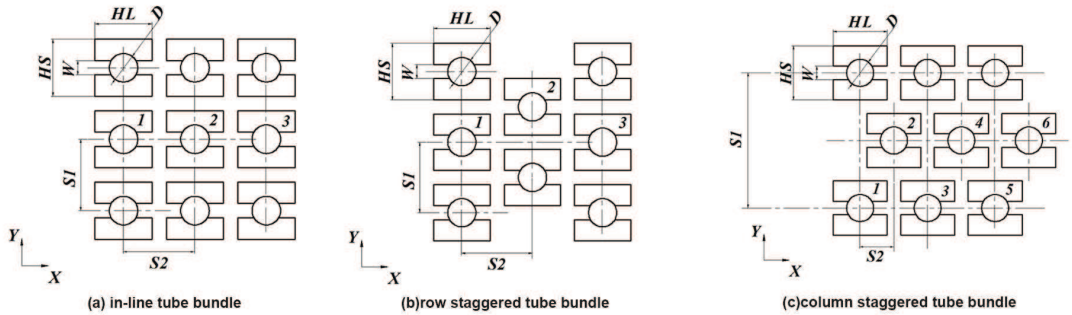

Figure 7: Schematic views of three H-type finned circular tube bundles.

Table 2: Geometric parameters of the six tube bundles.

Parameter	In-line	Row staggered	Column staggered
Tube diameter of circular tube, D (mm)	42	42	42
Larger ellipse diameter, a (mm)	52.5	52.5	52.5
Smaller ellipse diameter, b (mm)	30	30	30
Spanwise tube pitch, $S1$ (mm)	84	84	168
Longitudinal tube pitch, $S2$ (mm)	84	84	42
Fin thickness, Ft (mm)	1.5	1.5	1.5
Fin pitch, Fp (mm)	9	9	9
Fin height, HL (mm)	76.5	76.5	76.5
Fin width, HS (mm)	54	54	54
Number of tube rows, N	3	3	6

Fig. 8 presents the maximum penetration depth of each tube surface for the six tube bundles. It can be observed that for both the H-type finned circular tube surface and the H-type finned elliptic tube surface, the maximum penetration depths of the first tubes in in-line arrangement are exactly the same as that of the two staggered arrangements. For the in-line tube bundle, the most severe erosion occurs on the first tube while for both staggered tube bundles, the most severe erosion occurs on the second tube. It should be noted that as far as the anti-erosion ability is concerned, the column-staggered arrangement behaves much better than that of row-staggered one, and the maximum penetration depth of the former is only about one seventh of the latter at the same operation condition.

The particle trajectories of the three tube bundles for H-type finned circular/elliptic tube are shown in Fig. 9. Following features should be noted. For the in-line tube bundles, the particles colliding with the second tube are quite few under the protection of the first tube. However, for the two staggered tube bundles, the second tubes are collided not only by the particles rebounded from the first tube but also directly by the particles in the main stream. For the row staggered tube bundle, the average air flow velocity

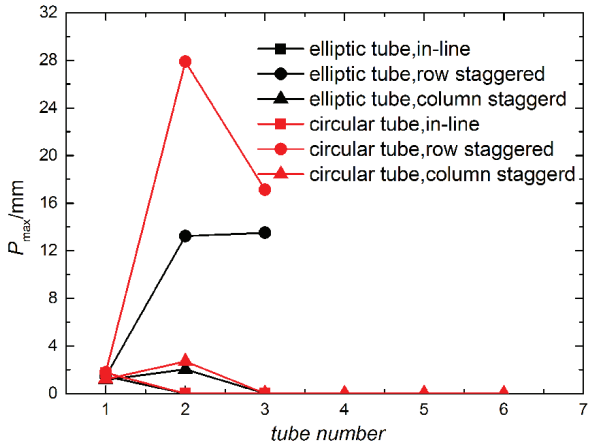

Figure 8: Maximum penetration depth of each tube surface.

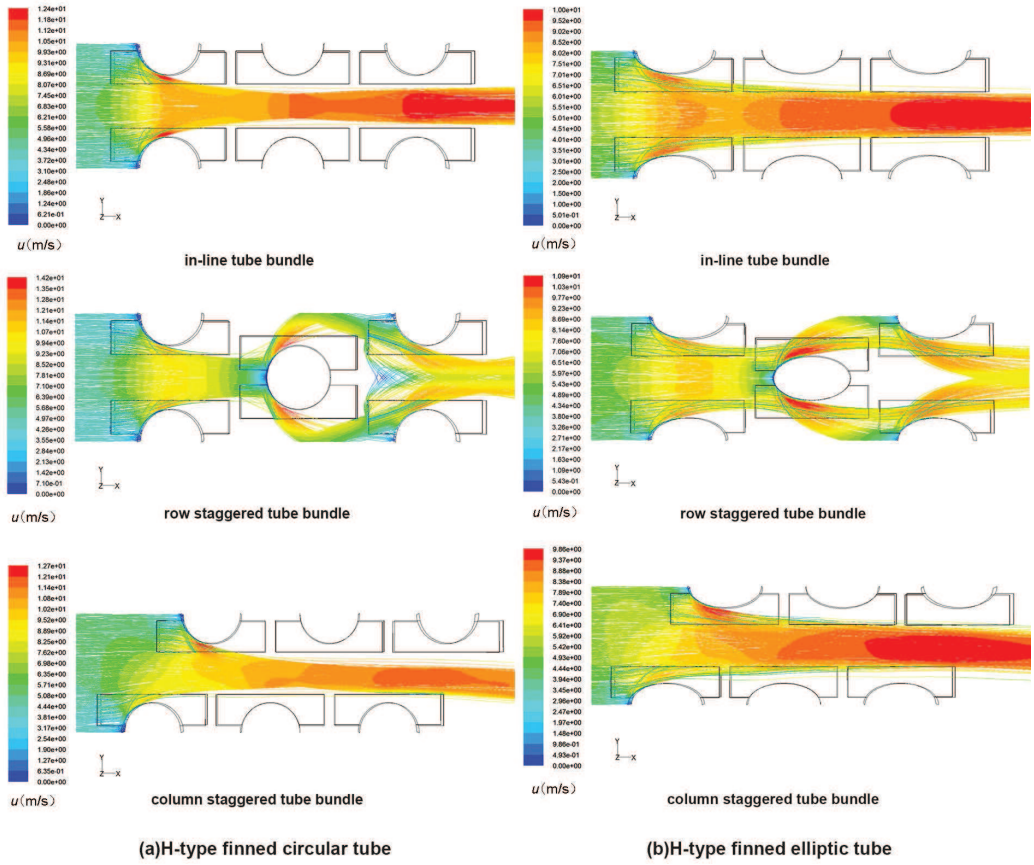

Figure 9: Comparison of particle trajectories in in-line, row staggered and column staggered tube bundles.

in the tubes is much bigger than that of the other two bundles, thus the maximum erosion of tube surface is most severe. Overall, from the view of reducing particle impact erosion, in-line tube arrangement has several advantages over the other two staggered tube arrangements, therefore it is widely used in the heat exchangers of waste heat recovery. Moreover, for the in-line tube arrangement, the most severe erosion occurs on the first row tube. Considering this, the following results are obtained for single row tube bundle.

3.2.2 The effect of particle size

For investigating the effects of particle size on the maximum penetration depths of H-type circular/elliptic tube surface, the particle size varied from 10μm to 100μm in the simulation. The other parameters remained the same as the basic prediction conditions in Table 1. The Reynolds number is set as 14400. It should be noticed that in order to study the influences of the parameters, the numerical simulations were always performed with $Re=14400$ and with one parameter varying in a certain range and the other parameters remained the same as the basic prediction conditions shown in Table 1. Moreover all dimensionless geometry parameters are based on the tube outside diameter (42mm) for circular tube and equivalent diameter (42mm) for elliptic tube. This will not be reaffirmed for simplicity.

First, some typical particle trajectories for different size of particles flowing past single row H-type finned circular tube surface are presented in Fig. 10. It can be observed that the trajectories of particles with different sizes are significantly different. In Fig. 10(a), the particles of diameter 10μm rarely collide with the tube surfaces. They are completely entrained by the fluid flow due to their low inertia. With the increase of particle size, an increasing number of particles strike on tube surfaces. Because the inertia of particles increases with the increase of particle diameter, the rebound phenomenon becomes increasingly significant. It can be observed that an immense difference among different size particle trajectories in the single row tubes. The smaller particles ($D_p \leq 50\mu$m) impact only one tube surface facing the oncoming flow while the larger particles ($D_p \geq 100\mu$m) also impact the other part of tube surface after rebounding. The effects of particle size on the maximum penetration depths of the single row H-type finned circular/elliptic tube surface are shown in Fig. 11. From Fig. 11 it can be seen that the maximum penetration depth of H-type finned elliptic tube surface is much smaller than that of H-type finned circular tube surface. It is due to the air flow velocity between the tube bundles of the H-type finned elliptic tube is lower than that of the H-type finned circular tube. Using H-type finned elliptic tube could effectively reduce the erosion rate of the tube surface. The other major feature observed from Fig. 11 is that the maximum penetration depth increases sharply with the increase of particle size when the particle size is less than 50 micrometers and increases mildly when it is larger than 50 micrometers. The trend is kept up to particle size of 100μm. The similar variation trend of erosion rate with particle size can be obtained in Ref. [16]. This feature can be illustrated as follows. In the condition of fixed particle concentration, the increase of particle size leads to an increase

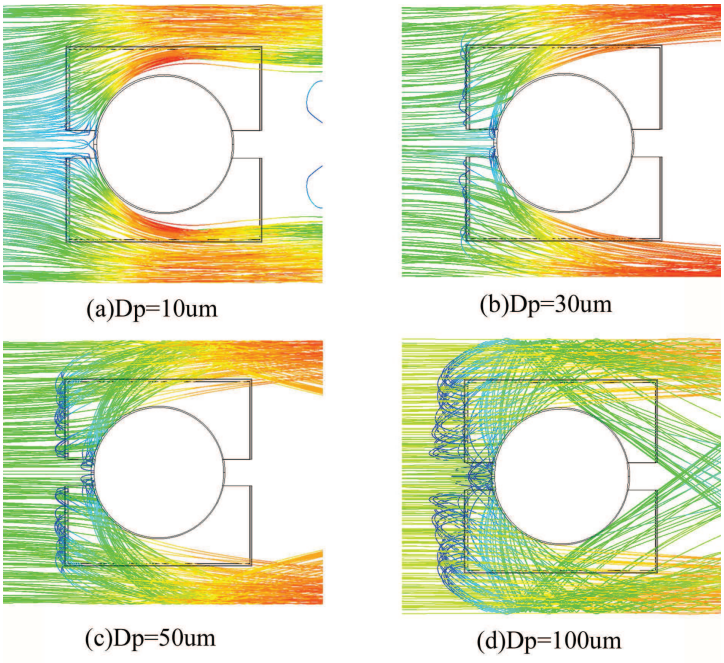

Figure 10: Typical particle trajectories for different size particles around a single row H-type finned circular tube surface.

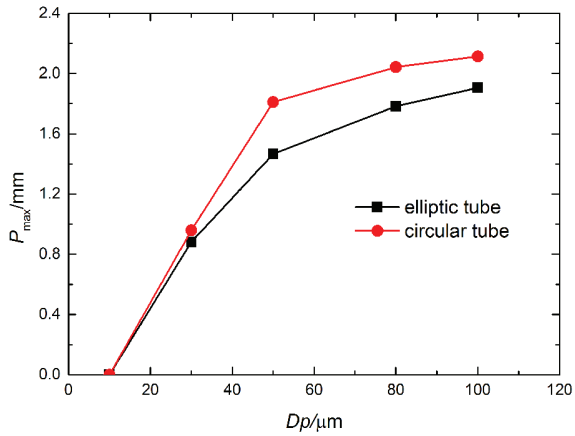

Figure 11: The effects of particle size on the maximum penetration depth of H-type finned circular/elliptic tube surface.

in kinetic energy of a single particle and a decease of total particle number in the gas flow. These two factors have the opposite effect on the tube erosion. When the particle size is less than 50μm, the first effect is predominant; when the particle size is larger than 50μm, the second effect becomes more important, largely compensating the effect of the first factor. Therefore, the erosion of tube surface could be reduced by decreasing the

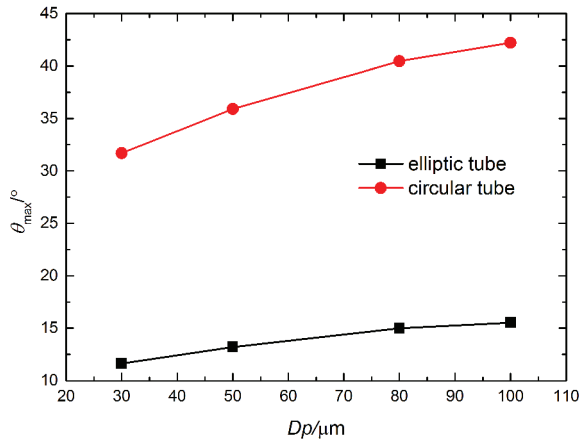

Figure 12: The effects of particle size on the location of maximum erosion of H-type finned circular/elliptic tube surface.

size of ash particles. Fig. 12 presents that the locations of maximum erosion on H-type finned circular/elliptic tube surface increase with the increase of ash particles' size and the increasing trends are gradually weakened.

3.2.3 The effect of particle concentration

The effects of particle concentration on the maximum penetration depths of the tube surface are examined within a variation range of particle concentration from 15g/m^3 to 37g/m^3 during the simulation. The effects of particle concentration on the maximum penetration depths of H-type finned elliptic/circular tube surface are shown in Fig. 13.

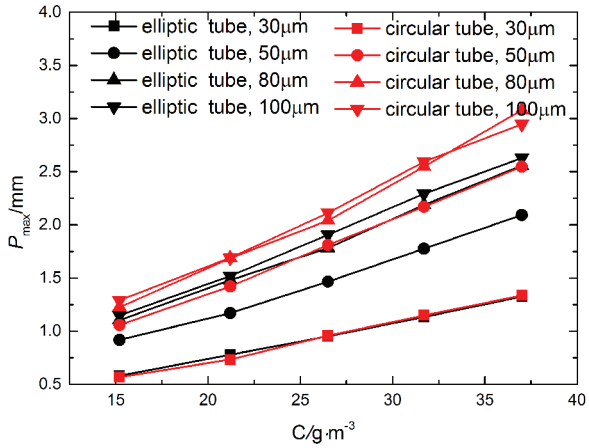

Figure 13: The effects of particle concentration on the maximum penetration depth of H-type finned circular/elliptic tube surface.

It can be observed that with the increase of particle concentration, the maximum penetration depths increase almost linearly. It implies that within the concentration range studied, the number of the particles actually impacting the tube surface increases proportionally with the increase of the particle concentration.

3.2.4 The effect of fluid Reynolds number

To study the effects of *Re* number on the maximum penetration depths of H-type finned circular/elliptic tube surface simulations are conducted for the inlet velocity from 3 to 7m/s, corresponding to a variation range of *Re* from 8600 to 20000. Fig. 14 presents the relations between the maximum penetration depth and *Re* number. With the increase of *Re* number, the maximum penetration depths increase, for the inlet velocity increases, the particles have a larger impact velocity and collision frequency. From curve-fitting of the numerical data, it can be observed that the maximum penetration depths are proportional to *Re* to the power 3.22-3.82. The results show good agreement with the test data in Ref. [7], which suggested that the erosion damage of tube is proportional to the oncoming velocity to the power 3.30-3.78. In Fig. 15, the variations of the location of maximum erosion H-type finned circular/elliptic tube surface with *Re* are presented, which implies that with the increase of *Re* the locations of maximum erosion H-type finned circular/elliptic tube surface increase. This effect of oncoming velocity on the penetration depth is nearly in its power of 3.5, which indicates that reduction of the oncoming velocity is a very effective method for reducing tube erosion.

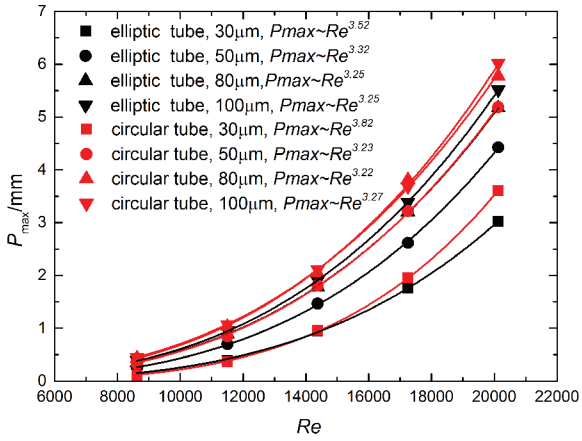

Figure 14: The effects of *Re* number on the maximum penetration depth of H-type finned circular/elliptic tube surface.

3.2.5 The effects of geometric parameters of H-type finned tube surface

For investigating the influences of geometric parameters of H-type finned circular/elliptic tube surface on the maximum penetration depth of the tube surface, simulations are performed for the dimensionless fin thickness from 0.024 to 0.071, the dimensionless fin

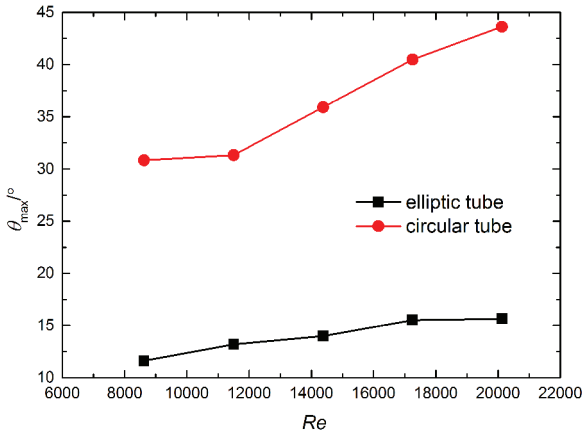

Figure 15: The effects of Re number on location of the maximum erosion of H-type finned circular/elliptic tube surface.

pitch from 0.17 to 0.36, the dimensionless fin length from 1.55 to 2.02, the dimensionless fin width from 1.19 to 2.67, the dimensionless slit width from 0.14 to 0.38 and the dimensionless transverse tube pitch from 1.55 to 2.26 respectively.

In Fig. 16(a)the variations of maximum penetration depths of H-type finned circular/elliptic tube surface with fin thickness are presented, which implies that with the increase of fin thickness the maximum penetration depth increases. Fig. 17 presents a schematic view of cross section normal to the oncoming flow, and Fig. 18 shows that with the increase in fin thickness the averaged flow velocity in both the areas A and B increases, leading to a higher velocity of the particles impacting on the tube wall. The relations between the maximum penetration depth and fin pitch are provided in Fig. 16(b). The maximum penetration depths of H-type finned circular/elliptic tube surface decrease with the increase of fin pitch. It is due to the fact that the average air flow velocity in the fin coil deceases with the increase of fin pitch. The effects of fin length on maximum penetration depths of tube surface are presented in Fig. 16(c). It can be observed that the maximum penetration depths increase with the increase of the fin length. It is because that when the air flows in the fin coil, the velocity of air flow is enhanced. Considering the inertia of the ash particles, the ash particles will be accelerated by the air flow. As a result, the longer the length of the fin is made, the greater the particles are accelerated to impact against the tube surface. Fig. 16(d) shows that the maximum penetration depths of H-type finned circular/elliptic tube surface increase with the increase of fin width. The average air flow velocity in the fin coil increases with the increase of fin width, which leads to the fact that the maximum penetration depths increase with the increase of fin width. The relations between the maximum penetration depth of H-type finned circular/elliptic tube surface and slit width are presented in Fig. 16(e). It can be observed that the flue gas velocity in the fin coil decreases with the increase of the slit width, which leads to the decrease of maximum penetration depths of H-type

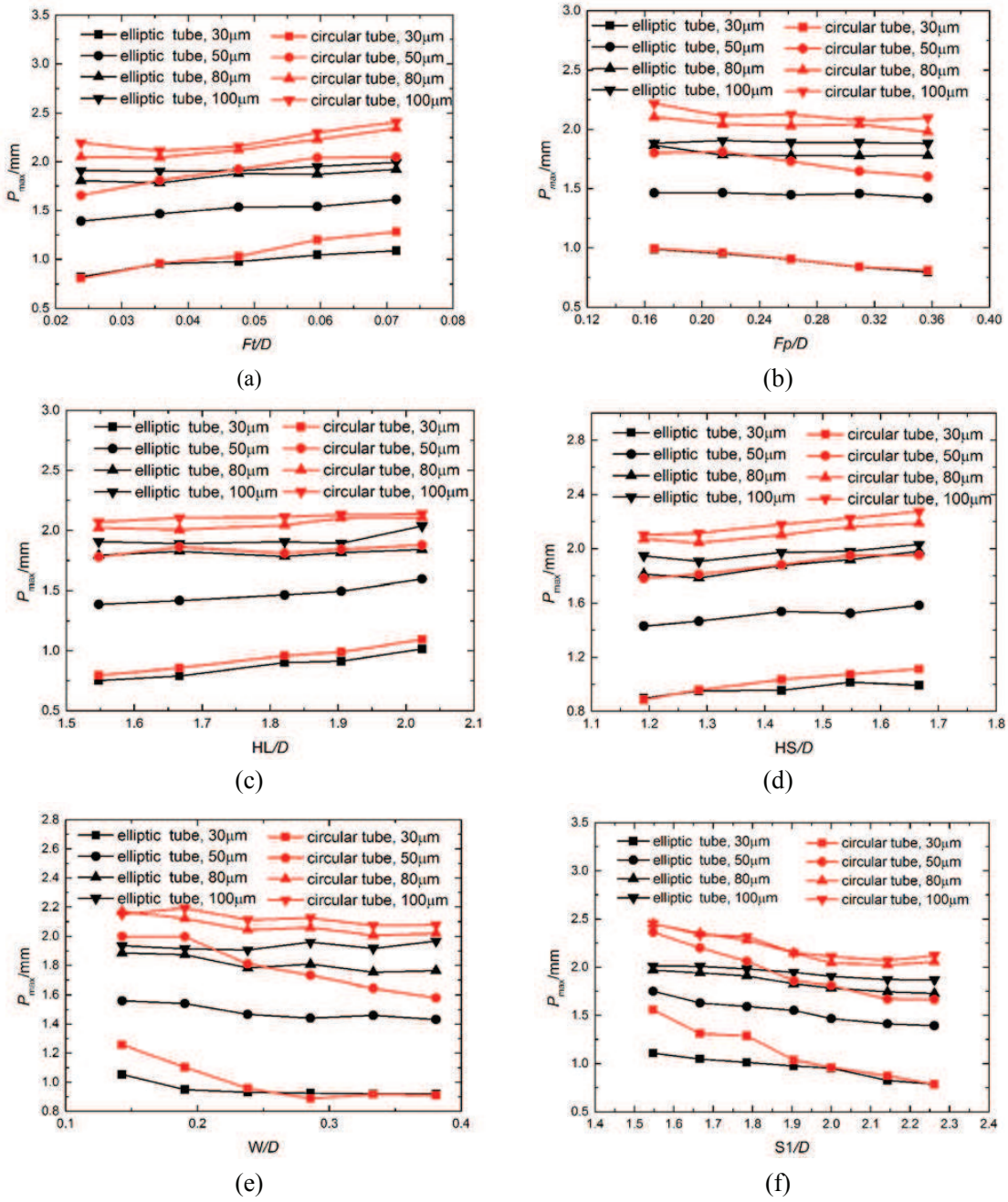

Figure 16: The effect of geometric parameters on the maximum penetration depth of H-type finned circular/elliptic tube surface: (a) fin thickness; (b) fin pitch; (c) fin height; (d) fin width; (e) slit width; (f) spanwise tube pitch.

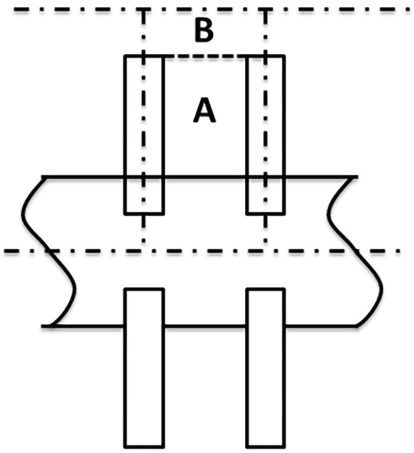

Figure 17: Illustration of effect of fin spacing.

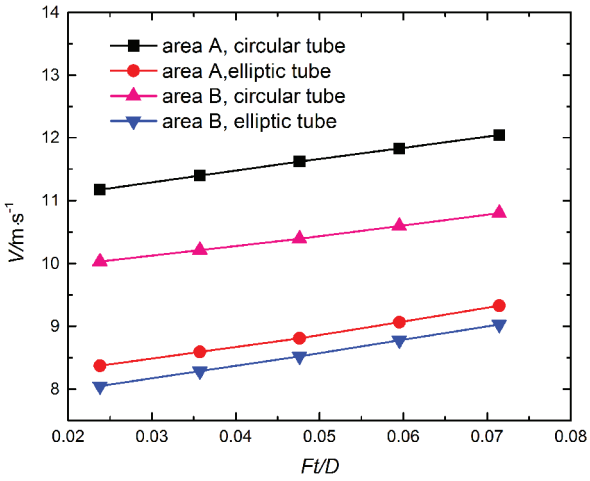

Figure 18: Average flow velocity in area A and B of H-type finned circular/elliptic tube surface.

finned circular/elliptic tube surface. The effects of the transverse tube pitch on the maximum penetration depths of H-type finned circular/elliptic tube surface can be observed in Fig. 16(f). With the increase of the transverse tube pitch, the maximum penetration depths of tube surface decrease. It is due to the fact that with the increase of the transverse tube pitch, the velocity of particles in the fin coils decreases. From Fig. 16(a) to Fig. 16(f), a common feature can be observed: the effects of geometric parameters of H-type finned circular/elliptic tube surface on the maximum penetration depths of the tube surface would be reduced with the decrease of particle size, because of the decrease of the particle inertia with particle size.

By investigating the effects of six geometry parameters on the erosion characters, it

can be demonstrated that the most influential parameter is transverse tube pitch, and the least influential one is slit width, with fin thickness, fin pitch, fin length and fin width in between.

4 Conclusion

In this paper, three-dimensional numerical simulations of solid particle erosion phenomena on H-type finned circular/elliptic tube surface are performed by software FLUENT. The geometry of tube surface is changed with the predicted erosion which is taken into account by a UDF and the flow field is re-solved for the eroded tube surface at every time step. The influences of ten parameters on the maximum erosion depth of the H-type circular/elliptic finned tube surface are well investigated. The following conclusions can be made:

1. H-type finned elliptic tube can reduce the penetration depth of tube surface compared with H-type finned circular tube.

2. The erosion in in-line tube arrangement is less severe than that in staggered tube arrangements. The column-staggered tube bank is less severe than that of staggered tube bank.

3. With the increase of particle size, particle concentration and fluid Reynolds number, the penetration depth of the tube surface increases. Especially the effect of fluid velocity is in the power of about 3.5.

4. Among the six geometric parameters, transverse tube pitch has the most important effect on the penetration depth of the H-type finned circular/elliptic tube surface.

The systematic numerical study on the erosion of H-type finned tube considering the deformation of tube surface introduced in this paper produces much more accurate result and plays a certain significant role in the anti-wear design of H-type finned tube heat exchanger.

Acknowledgments

This work is supported by the National Basic Key Research Program of China (973 Program, No. 2013CB228304).

References

[1] I. Finnie, Erosion of surfaces by solid particles, Wear, 3 (1960) 87-103.
[2] W. Tabakoff, R. Kotwal, A. Hamed, Erosion study of different materials affected by coal ash particles, Wear, 52(1) (1979) 161-173.

[3] W.P. Bauver, J.D. Bianca, J.D. Fishburn, J.G. Mcgowan, Characterization of erosion of heat transfer tubes in coal fired power plant, ASME Paper 84-JPGC-FU-3, 1984.
[4] K.P. Schade, H.J. Erdmann, T. Hadrich, H. Schneider, T. Frank, K. Bernert, Experimental and numerical investigation of particle erosion caused by pulverised fuel in channels and pipework of coal-fired power plant, Powder Technology, 125(2-3) (2002) 242-250.
[5] H.X. Li, T.K. Chen, H.F. Luan, Y.S. Luo, Y.P. Chu, Experimental research on the wear characteristics of heat transfer tubes in dusty gas flows, Power Engineering, 23(4) (2003) 2538-2542.
[6] T. Deng, M.S. Bingley, M.S.A. Bradley, The influence of particle rotation on the solid particle erosion rate of metals, Wear, 256(11-12) (2004) 1037-1049.
[7] J.R. Fan, D.D. Zhou, J. Jin, K. Cen, Numerical-simulation of tube erosion by particle impaction, Wear, 142(1) (1991) 171-184.
[8] J.Y. Tu, C.A.J. Fletcher, M. Behnia, Numerical modelling of three-dimensional fly-ash flow in power utility boilers, International Journal for Numerical Methods in Fluids, 24(8) (1997) 787-806.
[9] J.R. Fan, P. Sun, Y.Q. Zheng, X.Y. Zhang, K.F. Cen, A numerical study of a protection technique against tube erosion, Wear, 225 (1999) 458-464.
[10] B.E. Lee, C.A.J. Fletcher, M. Behnia, Computational study of solid particle erosion for a single tube in cross flow, Wear, 240(1-2) (2000) 95-99.
[11] J. Jin, J.R. Fan, X.Y. Zhang, K.F. Cen, Numerical simulation of the tube erosion resulted from particle impacts, Wear, 250 (2001) 114-119.
[12] B.E. Lee, J.Y. Tu, C.A.J. Fletcher, On numerical modeling of particle-wall impaction in relation to erosion prediction: Eulerian versus Lagrangian method, Wear, 252(3-4) (2002) 179-188.
[13] Z.F. Tian, J.Y. Tu, G.H. Yeoh, Numerical modelling and validation of gas-particle flow in an in-line tube bank, Computers & Chemical Engineering, 31(9) (2007) 1064-1072.
[14] Y. Liu, O. Hinrichsen, Numerical simulation of tube erosion in a bubbling fluidized bed with a dense tube bundle, Chemical Engineering & Technology, 36(4) (2013) 635-644.
[15] Z.L. Wang, J.R. Fan, K. Luo, Numerical study of solid particle erosion on the tubes near the side walls in a duct with flow past an aligned tube bank, Aiche Journal, 56(1) (2010) 66-78.
[16] K. Luo, F. Wu, K. Qiu, Z. Wang, J. Fan, Effects of preferential concentration on collision and erosion between solid particles and tube bank in a duct flow, International Journal of Heat and Mass Transfer, 83 (2015) 372-381.
[17] X.B. Zhao, G.H. Tang, X.W. Ma, Y. Jin, W.Q. Tao, Numerical investigation of heat transfer and erosion characteristics for H-type finned oval tube with longitudinal vortex generators and dimples, Applied Energy, 127 (2014) 93-104.
[18] Y. Wang, X. Zhao, G. Tang, Iop, Heat transfer, erosion and acid condensation characteristics for novel H-type finned oval tube, in: 7th International Conference on Cooling & Heating Technologies, 2015.
[19] F. Incorporated, Fluent 6.3.26 User's Guide, Fluent Incorporated Lebanon, NH, USA, 2006.
[20] W.Q. Tao, Numerical Heat Transfer, second edition, Xi'an Jiaotong University Press, Xi'an China, 2001.
[21] V. Yakhot, S.A. Orszag, Renormalization group analysis of turbulence. I. Basic theory, Journal of Scientific Computing, 1(1) (1986) 3-51.
[22] K.C. Cen, J.R. Fan, Theory and Calculation of Engineering Gas-Solid Multiphase Flow, Zhejiang University Press, Zhejiang, China, 1990.
[23] P.G. Saffman, The lift on a small sphere in a slow shear flow, Journal of Fluid Mechanics, 22 (1965) 385-400.

[24] M. Sommerfeld, N. Huber, Experimental analysis and modelling of particle-wall collisions, International Journal of Multiphase Flow, 25(6-7) (1999) 1457-1489.
[25] J.R. Fan, J. Yao, X.Y. Zhang, K.F. Cen, Experimental and numerical investigation of a new method for protecting bends from erosion in gas-particle flows, Wear, 251 (2001) 853-860.
[26] Y.Y. Niu, J.C. Tsao, Numerical evaluation of erosion in curved ducts, Numerical Heat Transfer Part A—Applications, 41(4) (2002) 341-356.